2015

Magnetic resonance imaging and histology correlation in the neocortex in temporal lobe epilepsy.

Maged Goubran

Robert R Hammond

Sandrine de Ribaupierre

Jorge G Burneo

Seyed Mirsattari

See next page for additional authors

Authors
Maged Goubran, Robert R Hammond, Sandrine de Ribaupierre, Jorge G Burneo, Seyed Mirsattari, David A Steven, Andrew G Parrent, Terry M Peters, and Ali R Khan

MRI and histology correlation in the neocortex of temporal lobe epilepsy

Maged Goubran [1,2,*], Robert R. Hammond [4], Sandrine de Ribaupierre [3], Jorge G. Burneo [3], Seyed Mirsattari [3], David Steven [3], Andrew G. Parrent [3], Terry M. Peters [1,2,5], Ali R. Khan [1,5]

[1] Imaging Research Laboratories, Robarts Research Institute,

[2] Biomedical Engineering Graduate Program,

[3] Epilepsy Program, Department of Clinical Neurological Sciences,

[4] Department of Pathology, Division of Neuropathology,

[5] Department of Medical Biophysics,

Western University, London, Ontario, Canada

* Corresponding author

Maged Goubran

mgoubran@robarts.ca

(519) 719-6705

P.O Box 5015 1151 Richmond St. North, London,

Ontario, Canada, N6A 5B7

Running Title

MRI-histology correlation in focal epilepsy

Number of characters in title: 72
Number of characters in running title: 44
Number of Figures: 7
Number of colour figures: 5
Word count (abstract): X
Word count (manuscript): X
Number of tables: 3

Abstract

Objective

To investigate the histopathological correlates of quantitative relaxometry and DTI and determine their efficacy in epileptogenic lesion detection for pre-operative evaluation of focal epilepsy.

Methods

We correlated quantitative relaxometry and DTI with histological features of neuronal density and morphology in 55 regions of the temporal lobe neocortex, selected from 13 patients who underwent epilepsy surgery. We made use of a validated non-rigid image registration protocol to obtain accurate correspondences between in-vivo MRI and histology images.

Results

We found T1 to be a predictor of neuronal density in the neocortical GM using linear mixed effects models with random effects for subjects. FA was a predictor of neuronal density of large-caliber neurons only (pyramidal cells, layers 3/5). Comparing multivariate to univariate mixed effects models with nested univariate demonstrated that employing T1 and FA together provided a significantly better fit than T1 or FA alone in predicting density of large-caliber neurons. Correlations with clinical variables revealed significant positive correlations between neuronal density with age ($r_s = 0.726$, $p_{fwe} = 0.021$). This study is the first to relate in-vivo T1 and FA values to the proportion of neurons in GM.

Interpretation

Our results suggest that quantitative T1 mapping and DTI may have a role in pre-operative evaluation of focal epilepsy and can be extended to identify gray matter pathology in a variety of neurological disorders.

Key words

Temporal lobe epilepsy, MRI, histology, correlation, relaxometry, neuronal density

Introduction

Approximately 30% of epileptic patients do not achieve remission with drugs [1]. Temporal lobe epilepsy (TLE) is the most common form of intractable focal epilepsy 2 and for many of these patients the standard of care is surgical treatment. A randomized controlled trial has shown this to be an effective treatment 3. However, seizure outcomes following surgical resection remain suboptimal, with a recent long-term study demonstrating that only half of such patients are seizure-free after 10 years 4. It is believed that early seizure recurrence is due to inadequate identification or removal of the epileptic lesion(s) or network 5, which may suggest the presence of dual pathology (histological abnormalities in the neocortex of patients with hippocampal sclerosis) or error in localising subtle neocortical lesions. However, whether these residual abnormalities are epileptogenic, or instead are the result of recurrent seizures, is still unclear. 1.1

In addition to electroencephalography, MRI can identify lesions related to seizure onset, and surgical outcomes are more favorable if an underlying lesion can be detected [6, 7]. However, clinical protocols for pre-operative assessment of focal epilepsy lack sensitivity, with more than 30% of patients diagnosed as MRI negative [8, 9], and the histological evaluation often reveals reactive changes or malformations of cortical development (MCD) [10,11]. Quantitative MRI sequences and image processing techniques such as T2 relaxometry mapping, diffusion tensor imaging (DTI), voxel-based morphometry and cortical thickness can reveal subtle pathologies undetected on routine MRI [12, 13, 14].

Imaging-histopathological correlations studies from neocortical specimens in TLE have been used to better understand the relationships between the two. Garbelli et al. (2012) [15]

demonstrated that blurred cortical boundaries in the temporal pole is correlated to degeneration of fibre bundles. With visually-matched ROIs, Eriksson et al. (2007) [16] found a negative correlation between GM fast FLAIR T2 (FFT2) and neuronal nuclear antigen (NeuN). A follow-up study [17] investigating GM probability maps with NeuN and glial fibrillary acidic protein (GFAP) did not find any correlations. Similarly, another study [18] also incorporating FLAIR and DTI still failed to find any correlations. Such data suggest that the pathological basis of abnormal MRI signals is poorly understood in focal epilepsy. The study and identification of quantitative imaging correlates relating to neocortical abnormalities can potentially reveal the association between these specific MRI parameters and seizure outcomes in MRI-negative patients. It would allow, as well the investigation of their effects on long-term surgical outcomes of patients with hippocampal sclerosis. 1.1

To this end, the objective of this work is to investigate the histopathological correlates of quantitative relaxometry and DTI from neocortical specimens of intractable TLE patients. We make use of a validated non-rigid image registration protocol to obtain accurate correspondences between quantitative in-vivo MRI and histology images. We first sample quantitative histology parameters from the gray and white matter in each NeuN (representing neuron integrity) and GFAP (representing gliosis) slide, and then use image registration to obtain the corresponding MRI parameters from high-resolution quantitative T1 and T2 maps along with DTI. 1.1

Materials and methods

Patients and Samples

2.1

Our study cohort included **13** TLE (5 males, 8 females, age: 34±15 (range: 18-56)) who underwent anterior temporal lobectomy (ATL) surgery. This project, part of an ongoing research study at the Robarts Research Institute, was approved by the office of research and ethics of Western University, and informed consent was obtained from all patients prior to their recruitment in the study. Patients had preoperative investigations including neuropsychological testing and 1.5T clinical MRI scans, which included T1-weighted, T2-weighted, FLAIR, and diffusion-weighted sequences. Patients were monitored with video-scalp EEG telemetry for seizure characterization, with three patients requiring subdural electrodes placement. In addition to the 1.5T clinical MRI scans performed as part of their clinical diagnosis, patients underwent a series of scans on a 3T MRI research scanner as described in the *in-vivo* MRI imaging subsection. Table 1 summarizes the age at the time of the last consultation prior to surgery, gender, age at seizure onset, electrographic seizure origin as well as clinical MRI and pathology findings for our patient cohort.

In-vivo Magnetic Resonance Imaging

All patients underwent pre-operative imaging, comprising relaxation mapping and DTI, on a 3 Tesla Discovery MR750 scanner (General Electric, Milwaukee, WI, U.S.A.) with a 32 channel head coil. For T1 mapping we employed the DESPOT1-HIFI approach [19] which involves the acquisition of two 3D SPGR sagittal T1-weighted image volumes (TR=8.36ms, TE=3.71ms, flip angles =4° & 18°, matrix=220x220, slice thickness=1mm, FOV=220 mm), as well as an additional inversion-prepared SPGR for B1 mapping (TR=6.4ms, TE=3.1ms, flip angle=5°, matrix=220x128, slice thickness=1mm, FOV=220 mm). For T2 mapping the DESPOT2-FM approach [20] was used, whereby five balanced steady-state free precession (bSSFP) images were

acquired with flip angles 5°, 35° and 68° with phase cycling patterns θ_{RF} = 0° and 180° (TR=4.6ms, TE=2.3ms, matrix=220x220, slice thickness=1, FOV=220 mm). DTI was performed using an axial spin-echo echo-planar imaging (EPI) sequence with 41 diffusion directions and a b-value of 1000 (TR=1100ms, TE=63.2ms, flip angle=90°, matrix=96x96, slice thickness=2.5, FOV=240 mm). To compute T1 and T2 quantitative maps, all the weighted images were registered to the first scan of the session using the FLIRT tool of the FSL image analysis suite (FSL, http://fsl.fmrib.ox.ac.uk) with an affine transformation to correct for motion between scans. T1 and T2 quantitative maps were subsequently reconstructed from their respective weighted images using their signal equations as described in (Deoni et al., 2007, 2009) [19, 20]. Eddy-current correction and diffusion tensor estimation were performed using FMRIB's Diffusion Toolbox (FDT) and maps of fractional anisotropy (FA), mean diffusivity (MD), radial diffusivity (RD) and axial diffusivity (AD) were transformed and resampled to the coordinate system defined by the 1mm isotropic T1 map.

Histological processing and quantitative histology

The specimens underwent accessioning and gross examination at the Department of Pathology at the University Hospital of London Health Sciences Centre, and were then bissected in the coronal plane. Each half of the specimen was embedded in agar for support and stabilization during slicing. The half-specimens were then sectioned, parallel to the initial cut, into 4.4 mm thick coronal slices using a commercial deli slicer. Each block was embedded in paraffin and sectioned at a thickness of 8 μm. Slides from each block were stained with hematoxylin and eosin (H&E) and processed for immunohistochemistry (IHC) to examine for NeuN (monoclonal antibody) and GFAP (polyclonal antibody) expression. Batch IHC processing was performed on

a Dako Autostainer Link 48 (Dako Corporation, Glostrup, Denmark) to minimize variability between slides. The resulting slides were digitized on a ScanScope GL (Aperio Technologies, Vista, CA, USA) bright field slide scanning system at a maximum of 20x optical zoom, and stitched to form full-frame multi-resolution images stored in BigTIFF file format (maximum pixel resolution 0.5 μm).

Field fraction estimates (proportion of all pixels in the field that were positively-stained) were used to quantify the NeuN and GFAP IHC. These estimates have been used in previous studies to represent neuronal integrity and gliosis [16, 17, 18] and are sensitive to the packing density and cell-size of neuronal cell bodies and processes (NeuN) or astrocytes (GFAP). The positive pixel count algorithm (Aperio Technologies, Vista, CA, USA) was employed for this purpose and employs color-based thresholding for hue, saturation, and intensity to determine whether or not a pixel is immuno-positive. Slides were batch processed using scripts written in MATLAB (The MathWorks Inc., Natick, MA, USA), processing the full resolution images in blocks of 100um x 100um. Hue and saturation thresholds were fixed (Hue value = 0.1, Hue width = 0.2 and saturation = $4x10^{-2}$) and the intensity threshold was chosen for each case to visualize the immuno-positive pixels and account for staining variability between slides.

Field fraction measurements involving dysplastic cortex could be less sensitive when reductions in packing density are accompanied by cyto-morphological size changes, since each would affect the field fraction in opposing directions. To better decouple these factors, we developed a method for segmenting the neuronal cell bodies to provide local estimates of neuron density and size. This procedure first employs colour deconvolution [21] to extract the colour

component related to immuno-positive staining, then performs a watershed-based segmentation procedure [22] for splitting joined or connected neurons, removes objects smaller than a predefined area defined as noise (less than 14 μm^2). This provides a segmentation of each individual neuron cell body that can be used to determine the neuron density in this field (# of neurons/field) and the mean size of neuron cell bodies in the field. To further discriminate between neurons, we also categorized them as either small-calibre (granular cells) or large-calibre (pyramidal cells) using an area threshold of 125 μm^2 and reported the density of each of these in the field. This procedure inherently allows analysis for laminar specificity since larger neurons are typically found in layers 3 and 5, and smaller neurons in layer 2 and 4. NeuN slides were batch-processed with scripts written in MATLAB, to extract the neuron-specific quantitative features in each 100μm x 100μm field. Figure 1 illustrates this procedure and demonstrates the six different quantitative histological features: NeuN field fraction, neuron density, mean neuron size, small neuron density, large neuron density, and GFAP field fraction.

ROI Placement and Image Registration

To quantitatively correlate in-vivo MRI parameters and corresponding histological features, we relied on region of interest (ROI) analysis as a means of extracting the desired parameters and features from homologous regions. Histology ROIs were delineated on 100 μm downsampled H&E histology slices using ITKsnap [23]. Since the middle temporal gyrus was present in all available resections, ROIs were defined on the histology slides at the crown of the gyrus comprising gray matter (GM) and white matter (WM) sub-regions (Figure 2), as was also done by Eriksson et al. (2007) [16]. The edges of the WM ROIs were constrained to be 2 mm from the gray/white boundary and were not delineated inside the high curvature regions of the gyrus. The

boundaries of the GM ROI were limited to a distance of 1mm from the pia to avoid partial volume effects on the in-vivo MRI images. A total of 55 ROIs: 29 GM and 26 WM (one patient had no WM ROIs as the resection did not include sufficient tissue), were segmented on histology slices. 2.1

To ensure that equivalent ROIs were analyzed in each modality, we employed non-rigid image registration to map the H&E defined histology ROIs to the IHC slides and the in-vivo MRI. Non-rigid image registration was performed between the in-vivo MRI and histology images, using an ex-vivo MRI scan of the specimen as an intermediate reference image to effectively split the registration in two steps. After surgical resection, each specimen was oriented by the operating neurosurgeon, photographed and transported on ice to the imaging lab for *ex-vivo* scanning, which was performed after overnight fixation in 10% formalin. Each specimen was wrapped in gauze for stabilization, transferred to suitably-sized containers for imaging, and immersed in a fluorine-based fluid 'Christo-lube MCG 1046' (Lubrication Technology, Inc) prior to imaging to avoid susceptibility artifacts at the tissue boundaries. The specimen scanning was performed on the same 3 T MR scanner employed for patient imaging, using a 6 channel coil designed to image the carotid artery. The sequences used for images that are part of the registration pipeline are described in detail below. The T2-weighted images were acquired with the fast imaging employing steady state acquisition (FIESTA) sequence (TR = 8.17ms, TE = 4.08ms, flip angle = 40°, N = 2, matrix = 200×200, slice thickness = 0.4, FOV = 70mm) with a resolution of 0.35 × 0.35 × 0.4mm. For cases where overnight imaging was feasible and not disruptive to the clinical workflow (N=4), scanning was performed on a 9.4T small bore Agilant MR magnet (Agilant, Santa Clara, CA, U.S.A) for improved image resolution

and signal-to-noise ratio (SNR), as an alternative to the 3T scan. The specimens were scanned with an in-house developed coil for a total time of sixteen hours. For this protocol, images were acquired with the TrueFisp sequence (TR = 7.6 ms, TE = 3.8 ms, flip angle = 30°) with an isotropic resolution of 0.2 mm and a FOV of (50×26×44) voxels.

First, we aligned the histology images from each specimen to the corresponding slice within the 3D ex-vivo MRI volume [25, 25]. Next, the in-vivo and ex-vivo MR images were aligned using a combination of image-based and landmark-based 3D deformable registration. The image-based registration made use of a B-spline deformation field and a normalized mutual information (NMI) cost-function [26], while the landmark registration relied on Gaussian radial basis functions [27]. Validation of our registration protocol was achieved by computing target registration error (TRE) based on manually-identified corresponding intrinsic anatomical landmarks, demonstrating registration errors of 0.98 ± 0.60 mm and 1.35 ± 0.11 mm for histology to ex-vivo and ex-vivo to in-vivo registrations respectively [24]. The IHC slides (NeuN and GFAP) were linearly co-registered to the H&E slides using downsampled grayscale images of each slide, with registration accuracy better than 0.5mm [25]. To avoid oblique resampling of the anisotropic histology images, for the purposes of visualization and analysis, the in-vivo and ex-vivo images were ultimately transformed to the space of the 3D reconstructed histology, *Hist3D*, where the reconstructed coronal histology slides are stacked parallel to the anterior-posterior axis. Figure 3 illustrates the four different spaces of MRI and histology, and registration results to bring both modalities in alignment. All in-vivo quantitative maps (T1, T2, FA, MD, AD and RD) were warped to the *Hist3D* space using the resultant deformation fields. Similarly, the histology ROIs were mapped to the IHC slides and the intermediate space, and underwent a final step of manual

correction, if needed, to account for potential registration errors and to circumvent partial volume effects. ROIs transformed to in-vivo MRI space were used to obtain estimates of the mean MRI parameter {T1, T2, FA, MD, AD, and RD} at each location in the plane corresponding to the histology slides.

Statistical analysis

To assess the Gaussianity of the distribution of MRI samples, we employed the D'agostino & Pearson omnibus normality test. Linear mixed effects with random effects were employed to test for relationships between MRI parameters and histological features. For these analyses the histological features (stain field fraction, neuron size and neuron counts) were entered as dependant variables and MRI parameters (T1, T2, FA, MD) from patients and slices as the independent variables, whereas variables for both patient and slice were entered as repeated measures. In addition, a random effect for subject was included to account for lower variance of MRI parameters within a single (across slices) subject as compared to between subjects. For fixed effects, we first fitted a model that included all MRI parameters as explanatory variables. We then used a backward elimination procedure to retain significant variables only. We employed Wald statistics for covariance structure selection. In addition, we assessed the correlations between each of the above variables as well as seizure frequency, age at the time of the last consultation prior to surgery, age of seizure onset, duration of epilepsy, and side of onset/resection. We also looked at correlations between each MRI parameter and every other MRI parameter, as well as those between histological features. We corrected for multiple comparisons in our correlation analysis with family-wise error rate (FWER) control using permutation tests [28], and the presented *p*-values are adjusted for family-wise error.

To investigate whether white matter MRI abnormalities are related to adjacent cortical histology, we also employed linear mixed models between MRI parameters from each WM ROI with histology features from its neighbouring GM ROI. Statistical analyses were performed in IBM SPSS statistics 20 (IBM, Armonk, NY). To test whether combining multiple MRI parameters leads to better prediction of histological features, multi-parametric models were compared against simpler univariate models using likelihood ratio tests.

Results

MRI parameters-Histology features correlation

The registration protocol enabled us to determine precise correspondences between MR and histology slices, and hence parameters from each slice were not averaged per patient and were instead employed as unique data points in the analysis. *P*-values from the linear mixed effects model analysis for the following histological features: neuron density, density (big neurons), density (small neurons), NeuN field fraction, are summarized in Table 2. T1 was found to be a significant predictor of total neuronal density in GM (Figure 4), as well as NeuN field fraction in the GM. Moreover, when assessing different sub-types of neurons, T1 and FA were both found to be predictors of neuronal density of large-caliber neurons (pyramidal cells) in the GM. Furthermore, only T1 was to be a predictor of small-caliber neurons (granular cells) in the GM. There were no significant associations between the GFAP field fraction and any MRI parameter in either GM or WM. Similarly, no significant associations were seen between histology and MRI parameters in the white matter.

Multivariate vs. univariate MRI

To test whether combining multiple MRI parameters leads to better prediction of histological features, multi-parametric mixed effects models were compared against nested univariate models using likelihood ratio tests and the chi-squared distribution. Multiple linear regression analysis demonstrated that combining T1 and FA values predicted GM neuronal density of large-caliber neurons with a better fit than T1 or FA on their own (-2 log likelihood difference: 12.06, $p < 0.001$). Other multi-parametric combinations however failed to demonstrate similar predictive improvements. Figure 5 plots the samples in the space spanned by T1 and FA, revealing that combining both parameters provides better discrimination of density of large neurons in neocortical GM. Each dot in this plot refers to a gray matter ROI on a histology slide, with representative dots being labeled with patient IDs from Table 1. It is clear from the figure that low and high neuron densities are not well separated when using T1 or FA (see projections on horizontal and vertical axes), but in the two-dimensional space the data are more clearly separable (demonstrated by the dashed line), suggesting that multivariate or multi-parametric analysis would be more beneficial in predicting or classifying pathology *in-vivo*. Since the presented ROIs are extracted from sparsely sectioned histology slices (4 mm apart), this figure highlights the potential of imaging parameters in detecting local pathology within the neocortex.

Correlation with clinical variables

2.1

Correlations with clinical variables revealed significant positive correlations between neuronal density and age ($r_s = 0.726$, $p_{fwe} = 0.021$). Finally there were significant correlations with side of seizure onset, with left TLE patients exhibiting increased GM T1 ($r_s = 0.671$, $p_{fwe} = 0.042$).

There were no correlations between clinical variables with MRI parameters and histological features in the white matter.

MRI-MRI parameters correlation

Table 3 summarizes the correlations between all MRI parameters within both tissue types (GM and WM). When assessing the relationships between diffusion and relaxometry parameters, there was a negative correlation between T1 and FA in WM, as well as a positive correlation between T1 values and MD in WM. When assessing the relationships between diffusion parameters (FA vs. MD) and relaxation parameters (T1 vs. T2) no significant correlations were found after multiple comparison correction. Figure 6 demonstrates the significant relationships between diffusion and relaxometry MRI parameters.

Histology-Histology features correlation

We found a positive correlation between neuronal density and NeuN field fraction in GM (r_s = 0.929, p = $4.0x10^{-09}$), as shown in Figure 6. Similarly, neuronal density was positively correlated with densities of both large and small neurons in GM when analyzed separately (r_s = 0.93, p = $1.4x10^{-09}$ and r_s = 0.95, p = $1.4x10^{-10}$). In addition, a slightly higher correlation was detected between NeuN field fraction and density of larger neurons in GM (r_s = 0.96, p = $1.5x10^{-11}$), than with density of smaller neurons in GM (r_s = 0.83, p = $1.8x10^{-05}$). Finally, the association between both measurements of densities proved positively correlated as well in GM (r_s = 0.80, p = $1.1x10^{-04}$).

Discussion

Neurobiological interpretations and considerations

A significant finding of this work was the negative association between T1 values and neuronal integrity measures (NeuN field fraction, neuronal density) in the gray matter. T1 relaxation is related to many factors in the tissue, including macromolecular integrity and the relationship between free and bound water. Neuronal loss will likely result in an overall loss of macromolecules and an increase in the extra-cellular space (thus increased amount of extra-cellular water and decreased amount of intra-cellular water), all of which would act to increase T1 [29]. A similar relationship between *ex-vivo* GM T1 values and neuronal density has been described in patients with multiple sclerosis [30]. Our study is the first to observe this relationship with *in-vivo* quantitative T1 mapping and in temporal lobe resections. Eriksson et al. (2007) [16] found correlations between T2 and gray matter NeuN field fraction, employing a dual-echo fast FLAIR T2 (FFT2) mapping at 1.5T with a 5 mm slice thickness. One possible explanation for why we did not observe this trend with our T2 maps is differences in the mapping protocols; our protocol at 3T, had significantly thinner slices, and did not use a fluid-attenuated inversion recovery (FLAIR) sequence. We plan to compare the relationship between our T1 and T2 maps and FLAIR sequences in future work to better understand the effectiveness of each technique in assessing pathology.

We also found that FA was a predictor of neuronal density of large-calibre (layer 3/5) neurons in the cortical gray matter. While this seems counterintuitive to our expectations in white matter, where a decrease in FA is usually associated with pathology, the cyto- and myelo-architecture in the cortex is considerably different from that in the white matter. Moreover, an increase in anisotropy was previously reported [31] within the dentate gyrus in an animal model of

seizing rats, as compared to naive controls. Diffusion anisotropy is low and not typically examined in the cortical gray matter, with some exceptions [32]. However high-resolution diffusion studies on post-mortem brains have shown that the fibre configuration can be complex, with both fibres parallel and perpendicular to the cortical surface observed, along with areas of fibre crossings [33]. In a region of low anisotropy due to fibre-crossing, such as the cortex, selective loss of one type of fibres would lead to an increase in anisotropy (i.e. a shift to a simpler fibre configuration). This phenomenon has been observed previously in a region of white matter fibre-crossing, where Douaud et al. (2011) [34] demonstrated an increase of FA could be explained by a relative preservation of motor-related projection fibres crossing the association fibres of the superior longitudinal fasciculus in subjects with mild cognitive impairment. Thus, the increase in FA we observed, coinciding with a loss of only large-calibre neurons, could be explained by the selective loss of fibres running either parallel or perpendicular to the cortical surface), as depicted in the simplified schematic representation in Figure 7. Given the limitations of *in-vivo* DTI data we cannot precisely assess the nature of the architectural changes related to FA, however we hope to explore these issues further using high-resolution ex-vivo DTI of the resected specimens. 1.2

In the white matter, increases in T1 were positively correlated with MD and negatively with FA. This agrees with previous studies that have also demonstrated reduced FA and increased MD in the ipsilateral white matter in TLE [35-39]. These changes may be due to degeneration of axons, reduced packing, or demyelination [40] which may facilitate isotropic diffusion and accumulation of free water in the extracellular space, which would lengthen T1 as well. A similar trend of prolonged T1 times and decreased FA was reported in white matter

hyperintense regions of Alzheimer's patients [41], where they showed that increased T1 reflected a range of pathological findings including axon and myelin loss and microglial activation, whereas the strongest predictor of decreased FA was axonal loss. In addition to affecting relaxation and diffusion parameters, reactive gliosis has also been previously associated with neuronal loss [42], however we did not observe any significant correlations with GFAP IHC in either GM or WM.

The positive correlation reported between age and neuronal density has been shown previously in a healthy aging population [43], and was attributed to atrophy (volume loss) without accompanied neuronal loss. This has potential implications on the detection of neuronal integrity, since if age-related atrophy (density increases) and neuron loss (density decreases) occur simultaneously, there may be no net change in density, and thus no change in MRI signal. Finally, we found significant differences in left-onset TLE patients, which had increased T1 and decreased FA in the gray matter. Asymmetry has also been found in other recent DTI studies [44, 45] with left-onset patients having more significant and widespread abnormalities and greater hippocampal atrophy [46], and have been speculated to be due to the greater vulnerability to early injury and the progressive effect of seizures on the left hemisphere. These asymmetric structural differences could also be related to the inherent functional lateralization, including language dominance [47].

2.1

Benefit of registration-based correlation

Many studies correlating MRI and histology have been performed without the use of computational methods for 3D image registration, relying instead on visual matching of ROIs. However, this is difficult in cases where the visibility or boundaries of the lesion in MRI and

histology differ and where no definitive lesion is apparent (as in paradoxical TLE). Another drawback of visual matching is that it becomes more challenging to find corresponding slices when there are 3D deformations present, as the anatomy in a histology slice may not be fully present in a single MRI slice, even if obliquely resampled. If no registration is employed and the tissue is subjected to non-rigid deformations, the samples from both modalities may represent different parts of the same anatomical region, which could potentially lead to abnormal sub-regions of one modality being correlated with normal elements of the other. When image registration is employed, the degree of mismatch between regions of both modalities becomes dependant on the registration error. For example, an image registration error between *in-vivo* MRI and histology of 1 mm would produce an overlap of 70% between two regions of interests with a volume of 140 mm^3 on each modalities, (roughly the size of a very small FCD) [48].

Limitations and future work

The current study is limited to the investigation of neuronal integrity and gliosis through field fractions and measurements of neuronal size and density. Since focal neuronal loss and gliosis are thought to be related to epileptogenicity, correlation of these measures with MRI is an important step in validating quantitative imaging techniques. Additional insight might also be gained through the use of myelin-specific stains (Luxol fast blue, or myelin basic protein), since their relationship with both T1 [49] and T2 [30] has been previously demonstrated. Another limitation of this work is the lack of normative control data for histology. Several post-mortem control neocortical specimens were acquired for histological analysis; however the staining ability of NEUN degrades with time after formalin fixation [50]. Moreover, it is logistically very difficult to obtain ethics approval for acquiring and handling fresh (unfixed) brain control specimens. We

plan to address these issues in future studies. The lack of control non-epileptic specimens makes it difficult to validate that the observed pathological changes directly relate to seizure generation, and hence the presented findings should be considered preliminary.

In addition to histopathology, correlation with electrophysiology obtained with intracranial EEG (iEEG) could be used to further validate these techniques and better understand the relationship with epileptogenicity, imaging, and histology. However, there are some issues with using iEEG as a gold-standard for validating imaging methods, since localization is limited to placement of the electrodes and abnormal iEEG may not actually have an altered structural substrate that can be detected. For these reasons, it may still be more beneficial to investigate the histopathological correlates instead of iEEG, specifically of cortical dysplasia, which often go undetected and have a higher risk for seizure recurrence [51]. We intend as well to correlate our imaging findings (specifically abnormalities found on T1 and FA maps) with long-term seizure outcomes, and investigate whether the absence of such lesions provides more favourable outcomes for MRI-negative patients, as well as patients undergoing surgery due to hippocampal sclerosis. Future work should as well investigate whether these neocortical abnormalities are related to the epileptogenicity in those patients, possibly though correlation of the imaging abnormalities with depth electrodes recordings on truly MRI-negative patients (those without any identifiable lesions whether in the hippocampus or neocortex). Better quantification and characterization of these lesions in histology, based on neuronal- and laminar-centric analysis, could be used to improve detection and precise delineation with MRI, and could improve surgical outcomes through more complete resection of the underlying pathology [52]. Our future

1.1

work in this direction will build upon histological image processing techniques and ex-vivo MR microscopy to accurately quantify and characterize these lesions for correlation with MRI.

Conclusion

In conclusion, we have demonstrated that alterations of in-vivo T1 and FA, in the temporal lobe cortex and white matter, are predictive of neuronal integrity (density and size) that serve to delineate an epileptogenic lesion. Our study is the first to quantitatively assess the relationship between MRI and histopathological features using correspondences based on image registration in focal epilepsy, and to relate in-vivo T1 and FA values to the proportion of neurons, specifically large-caliber neurons, in the neocortical gray matter. Our registration and correlation pipeline allows for a quantitative assessment of the pathological correlates of MRI by bringing information from both modalities, and the potential prediction of pathology from *in-vivo* MRI. This study suggests that quantitative MRI sequences, specifically multi-parameter T1 mapping and DTI, may have a role in routine clinical practice for pre-operative evaluation of focal epilepsy and motivates further investigation in this area. These in-vivo quantitative maps can be extended as well to identify gray matter lesions in multiple sclerosis or be used as a marker for degeneration in neurodegenerative diseases as Alzheimer's.

Acknowledgments

The authors would like to thank Cathie Crukley, Robert Mayer and Catherine Currie for their assistance and support throughout the study.

This project is funded by the Canadian Institute of Health Research (CIHR) grant MOP 184807 and Canada Foundation for Innovation (CFI) grant 20994. MG is supported by the NSERC Create Grant CAMI award at Western University. AK is supported by a post-doctoral fellowship from the Canadian Institute of Health Research (CIHR).

References

1. Engel J. Etiology as a risk factor for medically refractory epilepsy: A case for early surgical intervention. Neurology 1998;51:1243-1244.
2. Engel J. Mesial temporal lobe epilepsy: What have we learned? Neuroscientist 2001;7:340-352.
3. Wiebe S, Blume WT, Girvin J P, Eliasziw M. A randomized, controlled trial of surgery for temporal-lobe epilepsy. New England Journal of Medicine 2001;345:311-318.
4. de Tisi J, Bell GS, Peacock JL, McEvoy AW, Harkness WF, Sander JW, et al. The long-term outcome of adult epilepsy surgery, patterns of seizure remission, and relapse: A cohort study. The Lancet 2011;378:1388-1395.
5. Najm I, Jehi L, Palmini A, Gonzalez-Martinez J, Paglioli E, Bingaman W. Temporal patterns and mechanisms of epilepsy surgery failure. Epilepsia 2013;54:772-782.
6. Blume WT, Ganapathy GR, Munoz D, Lee DH. Indices of resective surgery effectiveness for intractable nonlesional focal epilepsy. Epilepsia 2004;45:46-53.
7. Jeha L, Najm I, Bingaman W, Khandwala F, Widdess-Walsh P, Morris H, et al. Predictors of outcome after temporal lobectomy for the treatment of intractable epilepsy. Neurology 2006;66:1938-1940.
8. Cohen-Gadol AA, Bradley CC, Williamson A, Kim JH, Westerveld M, Duckrow RB, et al. Normal magnetic resonance imaging and medial temporal lobe epilepsy: The clinical syndrome of paradoxical temporal lobe epilepsy. J Neurosurg 2005;102:902-909.

9. Sylaja P, Radhakrishnan K, Kesavadas C, Sarma P. Seizure outcome after anterior temporal lobectomy and its predictors in patients with apparent temporal lobe epilepsy and normal MRI. Epilepsia 2004;45:803-808.
10. Lee SK, Lee SY, Kim K, Hong K, Lee D, Chung C. Surgical outcome and prognostic factors of cryptogenic neocortical epilepsy. Ann Neurol 2005;58: 525-532.
11. Widdess-Walsh P, Diehl B, Najm I. Neuroimaging of focal cortical dysplasia. Journal of Neuroimaging 2006;16:185-196.
12. Bernasconi A, Bernasconi N, Caramanos Z, et al. T2 relaxometry can lateralize mesial temporal lobe epilepsy in patients with normal MRI. Neuroimage 2000;12:739-746.
13. Bernasconi N, Duchesne S, Janke A, Lerch J, Collins D, Bernasconi A. Whole-brain voxel-based statistical analysis of gray matter and white matter in temporal lobe epilepsy. Neuroimage 2004;23:717-723.
14. Bernhardt B, Worsley K, Kim H, Evans A, Bernasconi A, Bernasconi N. Longitudinal and cross-sectional analysis of atrophy in pharmacoresistant temporal lobe epilepsy. Neurology 2009;72:1747-1754.
15. Garbelli R, Milesi G, Medici V, Villani F, Didato G, Deleo F, et al. Blurring in patients with temporal lobe epilepsy: Clinical, high-field imaging and ultrastructural study. Brain 2012;135:2337-2349.
16. Eriksson S, Free S, Thom M, Martinian L, Symms M, Salmenpera T, et al. Correlation of quantitative MRI and neuropathology in epilepsy surgical resection specimens—T2 correlates with neuronal tissue in gray matter. Neuroimage 2007;37:48-55.

17. Eriksson SH, Free SL, Thom M, Symms MR, Martinian L, Duncan JS, et al. Quantitative gray matter histological measures do not correlate with gray matter probability values from in vivo MRI in the temporal lobe. J Neurosci Methods 2009;181:111-118.
18. Lockwood-Estrin G, Thom M, Focke NK, Symms MR, Martinian L, Sisodiya SM, et al. Correlating 3T MRI and histopathology in patients undergoing epilepsy surgery. J Neurosci Methods 2012;205:182-189.
19. Deoni SC. High-resolution T1 mapping of the brain at 3T with driven equilibrium single pulse observation of T1 with high-speed incorporation of RF field inhomogeneities (DESPOT1-HIFI). J Magn Reson Imaging 2007;26:1106-1111.
20. Deoni SC. Transverse relaxation time (T2) mapping in the brain with off-resonance correction using phase-cycled steady-state free precession imaging. J Magn Reson Imaging 2009;30:411-417.
21. Ruifrok AC and Johnston DA. Quantification of histochemical staining by color deconvolution. Anal Quant Cytol Histol. 2001;23(4):291-299.
22. Soille P. Morphological Image Analysis: Principles and Applications. Springer-Verlag New York, Inc; 2003.
23. Yushkevich PA, Piven J, Hazlett HC, Smith RG, Ho S, Gee JC, et al. User-guided 3D active contour segmentation of anatomical structures: Significantly improved efficiency and reliability. Neuroimage 2006;31:1116-1128.
24. Goubran M, Khan AR, Crukley C, Buchanan S, Santyr B, deRibaupierre S, Peters TM. Robust registration of sparsely sectioned histology to ex-vivo MRI of temporal lobe resections. Proc. SPIE 8314, Medical Imaging 2012;8314:83141V.

25. Goubran M, Crukley C, de Ribaupierre S, Peters TM, Khan AR. Image registration of ex-vivo MRI to sparsely sectioned histology of hippocampal and neocortical temporal lobe specimens. Neuroimage 2013;83:770-781.
26. Modat M, Ridgway GR, Taylor ZA, Lehmann M, Barnes J, Hawkes DJ, et al. Fast free-form deformation using graphics processing units. Comput Methods Programs Biomed 2010;98:278–284.
27. Pinter C, Lasso A, Wang A, Jaffray D, Fichtinger G. SlicerRT: Radiation therapy research toolkit for 3D Slicer. Medical physics 2012;39:6332-6338.
28. Groppe DM, Urbach TP, Kutas M. Mass univariate analysis of event-related brain potentials/fields I: A critical tutorial review. Psychophysiology 2011;48:1711-1725.
29. Jurcoane A, Wagner M, Schmidt C, Mayer C, Gracien R, Hirschmann M, et al. Within-lesion differences in quantitative MRI parameters predict contrast enhancement in multiple sclerosis. J Magn Reson Imaging 2013;38:1454-1461.
30. Schmierer K, Parkes HG, So P-, An SF, Brandner S, Ordidge RJ, et al. High field (9.4 tesla) magnetic resonance imaging of cortical gray matter lesions in multiple sclerosis. Brain 2010;133:858-867.
31. Parekh MB, Carney PR, Sepulveda H, Norman W, King M, Mareci TH. Early MR diffusion and relaxation changes in the parahippocampal gyrus precede the onset of spontaneous seizures in an animal model of chronic limbic epilepsy. Expr Neurol 2010;224:258-270.
32. Kang DH, Jo HJ, Jung WH, Kim SH, Jung YH, Choi CH, et al. The effect of meditation on brain structure: cortical thickness mapping and diffusion tensor imaging. Soc Cogn Affect Neurosci 2013;8:27-33.

522 33. Leuze CW, Anwander A, Bazin PL, Dhital B, Stüber C, Reimann K, et al. Layer-specific
523 intracortical connectivity revealed with diffusion MRI. Cereb Cortex 2014;24:328-339.
524 34. Douaud G, Jbabdi S, Behrens TEJ, Menje RA, Gass A, Monsch AU, et al. DTI measures in
525 crossing-fibre areas: Increased diffusion anisotropy reveals early white matter alteration in
526 MCI and mild Alzheimer's disease. Neuroimage 2011;55:880-890.
527 35. Rugg-Gunn FJ, Eriksson SH, Symms MR, Barker GJ, Thom M, Harkness W, et al. Diffusion
528 tensor imaging in refractory epilepsy. The Lancet 2002;359:1748-1751.
529 36. Focke NK, Yogarajah M, Bonelli SB, Bartlett PA, Symms MR, Duncan JS. Voxel-based
530 diffusion tensor imaging in patients with mesial temporal lobe epilepsy and hippocampal
531 sclerosis. Neuroimage 2008;40:728-737.
532 37. Salmenpera TM, Simister RJ, Bartlett P, Symms MR, Boulby PA, Free SL, et al. High-
533 resolution diffusion tensor imaging of the hippocampus in temporal lobe epilepsy. Epilepsy
534 Res 2006;71:102-106.
535 38. Thivard L, Lehéricy S, Krainik A, Adam C, Dormont D, Chiras J, et al. Diffusion tensor
536 imaging in medial temporal lobe epilepsy with hippocampal sclerosis. Neuroimage
537 2005;28:682-690.
538 39. Khan AR, Goubran M, de Ribaupierre S, Hammond RR, Burneo JG, Parrent AG, Peter TM.
539 Quantitative relaxometry and diffusion MRI for laterization in MTS and non-MTS temporal
540 lobe epilepsy. Epilepsy Research 2014;108:506-516.
541 40. Gross DW. Diffusion tensor imaging in temporal lobe epilepsy. Epilepsia 2011;52:32-34.
542 41. Gouw AA, Seewann A, Vrenken H, van der Flier WM, Rozemuller JM, Barkhof F, et al.
543 Heterogeneity of white matter hyperintensities in alzheimer's disease: Post-mortem
544 quantitative MRI and neuropathology. Brain 2008;131:3286-3298.

42. Block ML, Zecca L, Hong J. Microglia-mediated neurotoxicity: Uncovering the molecular mechanisms. Nature Reviews Neuroscience 2007;8:57-69.
43. Freeman SH, Kandel R, Cruz L, Rozkalne A, Newell K, Frosch MP, Hedley-Whyte ET, et al. Preservation of neuronal number despite age-related cortical brain atrophy in elderly subjects without Alzheimer disease. J Neuropathol Exp Neurol 2008;67(12):1205-1212.
44. Shon Y, Kim Y, Koo B, Lee J, Kim HJ, Kim WJ, et al. Group-specific regional white matter abnormality revealed in diffusion tensor imaging of medial temporal lobe epilepsy without hippocampal sclerosis. Epilepsia 2010;51:529-535.
45. Kemmotsu N, Girard HM, Kucukboyaci N E, McEvoy LK, Hagler DJ, Dale AM, et al. Age-related changes in the neurophysiology of language in adults: Relationship to regional cortical thinning and white matter microstructure. J Neurosci 2012;32:12204-12213.
46. Bonilha L, Rorden C, Halford, J J, Eckert M, Appenzeller S, Cendes F, et al. Asymmetrical extra-hippocampal gray matter loss related to hippocampal atrophy in patients with medial temporal lobe epilepsy. J Neurol Neurosurg Psychiatry 2007;78:286-294.
47. Barrick TR, Lawes IN, Mackay CE, Clark CA. White matter pathway asymmetry underlies functional lateralization. Cereb Cortex 2007;17(3):591-598.
48. Besson P, Bernasconi N, Colliot O, Evans A, Bernasconi A. Surface-based texture and morphological analysis detects subtle cortical dysplasia. In: Medical Image Computing and Computer-Assisted Intervention--MICCAI 2008;2008:645-652.
49. Mottershead J, Schmierer K, Clemence M, Thornton J, Scaravilli F, Barker G, et al. High field MRI correlates of myelin content and axonal density in multiple sclerosis. J Neurol 2003;250:1293-1301.

50. Lyck L, Dalmau I, Chemnitz J, Finsen B, Daa Schroder H. Immunohistochemical Markers for Quantitative Studies of Neurons and Glia in Human Neocortex. Journal of Histochemistry & Cytochemistry 2008;56:201-221.

51. Palmini A, Gambardella A, Andermann F, Dubeau F, da Costa JC, Olivier A, et al. Operative strategies for patients with cortical dysplastic lesions and intractable epilepsy. Epilepsia 1994;35:57–71.

52. Fauser S, Schulze-Bonhage A, Honegger J, Carmona H, Huppertz HJ, Pantazis G, et al. Focal cortical dysplasias: surgical outcome in 67 patients in relation to histological subtypes and dual pathology. Brain 2004;127:2406–2418.

Table 1. Patient demographics and clinical information including age, gender, onset age, seizure origin as well as clinical MRI and pathology findings for our patient cohort. MTS = mesial temporal sclerosis, MAA= minor architectural abnormalities, Neo. Path. = Neocortical Pathology, Hp. Path. = Hippocampal Pathology † Previous resection of left temporal lobe tumour (DNET), * not enough tissue to make diagnosis of MTS

Patient	Gender	Age	Age of Onset	Sz Origin	Sz Freq. /month	MRI	Neo. Path.	Hp. Path.	Engel outcome	Yrs since surger
1	F	25	17	L	2	Normal †	Gliosis, Ki67-positive cells in WM†	Gliosis	3	2.0
2	M	20	3	L	16	MTS	Gliosis, MAA	MTS	2	2.1
3	M	18	14	R	32	Possible MTS	Gliosis, MAA	Gliosis*	1	2.1
4	F	48	36	L	28	MTS	Gliosis	MTS	1	1.7
5	F	50	47	L	20	GM/WM blurring	Gliosis	Gliosis*	1	1.6
6	M	31	28	R	2	Normal	Mild gliosis, MAA	Negligible gliosis	1	1.3
7	F	32	19	L	2	MTS	Gliosis	MTS	1	1.2
8	F	43	3	R	4	MTS	Gliosis	MTS	2	1.4
9	F	26	19	R	12	Cortical tubers	Dysplastic lesion, cortical tuber	Gliosis	2	2.5
10	M	34	15	L	2	MTS	Gliosis, focal MAA	MTS	3	1.2
11	F	40	7	R	20	MTS, Porencephaly	Gliosis, MAA	MTS	2	2.5
12	F	56	15	R	8	Normal	Gliosis, arteriosclerosis	Gliosis*	1	1
13	M	23	18	L	12	Normal	Gliosis, MAA, possible FCD type 1a	Gliosis	1	1

Table 2. Results of the linear mixed-effects models with random effects for subjects, showing *p*-values for variables with significant fixed effects.

Grey matter	Neuron density	Neuron density (large neurons)	Neuron density (small neurons)	NEUN field fraction
T1	0.007	0.019	0.004	0.001
T2				
FA		0.009		
MD				

The minimum adequate model was obtained by backward selection removing the non-significant fixed effects.

Table 3. Significance of Spearman Rho correlations between MR parameters. All *p*-values were corrected for family wise error.

Grey matter parameters	**T1**	**T2**	**FA**	**MD**
T1		r = 0.323 P = 0.428	r = −0.207 P = 0.515	r = 0.129 P = 0.843
T2			r = −0.316 P = 0.463	r = −0.036 P = 0.931
FA				r = −0.188 P = 0.612
MD				
White matter parameters	**T1**	**T2**	**FA**	**MD**
T1		r = 0.464 P = 0.144	r = −0.806 **P = 1.73e-04***	r = 0.643 **P = 0.032**
T2			r = −0.229 P = 0.639	r = 0.381 P = 0.241
FA				r = −0.527 P = 0.147
MD				

Figure legends

Figure 1. Histological processing and semi-quantitative features extraction, for both NeuN and GFAP IHC stains.

Figure 2. ROI placement and MRI parameters extraction. **A)** Gray matter and white ROI on 100um H&E histology slice in histology native space. **B)** Registered *ex-vivo* MRI slice corresponding to the histology slice in *Hist3D* space. **C)** Warped ROIs overlaid on the registered and obliquely resampled T1 map in *Hist3D* space where MRI parameters extraction is performed. The registered histology slice is shown in the top left corner. **D)** Warped ROIs in the native *in-vivo* MRI space overlaid on three consecutive slices of the T1 map for illustration purposes.

Figure 3. Overview of our registration pipeline depicting registration results and the four different spaces of MRI and histology including the intermediate *Hist 3D* space where reconstructed histology slices are stacked parallel to the A-P axis.

Figure 4. Relationships between quantitative MRI parameters (T1 and FA) and neuronal density in GM (Top left: Total neuronal density, Top right: Neuronal density for small-caliber neurons, Bottom: Neuronal density for large-caliber neurons).

Figure 5. Representation of T1-FA multi-parametric space, revealing that combining T1 and FA provides better discrimination of normal and abnormal neuron density in neocortical gray matter. Each dot in this plot refers to a gray matter ROI on a histology slide, with representative dots being labeled with patient IDs from Table 1. It is clear from the figure that low and high neuron densities are not well separated when using T1 or FA (see projections on horizontal and vertical axes), but in the two-dimensional space the data demonstrate are more clearly separable (demonstrated by the dashed line), suggesting that multivariate or multi-parametric analysis

would be more beneficial in predicting or classifying pathology *in-vivo*. Since the presented ROIs are extracted from sparsely sectioned histology slices (4 mm apart), this figure highlights the potential of imaging parameters in detecting local pathology within the neocortex.

Figure 6. Significant relationships between diffusion and relaxometry MRI parameters, as well as the association between neuronal density and NeuN field fraction.

Figure 7. Summary of MRI parameters and histological features correlations in both tissues of the temporal lobe neocortex, along with possible neurobiological explanations for the highlighted relations.

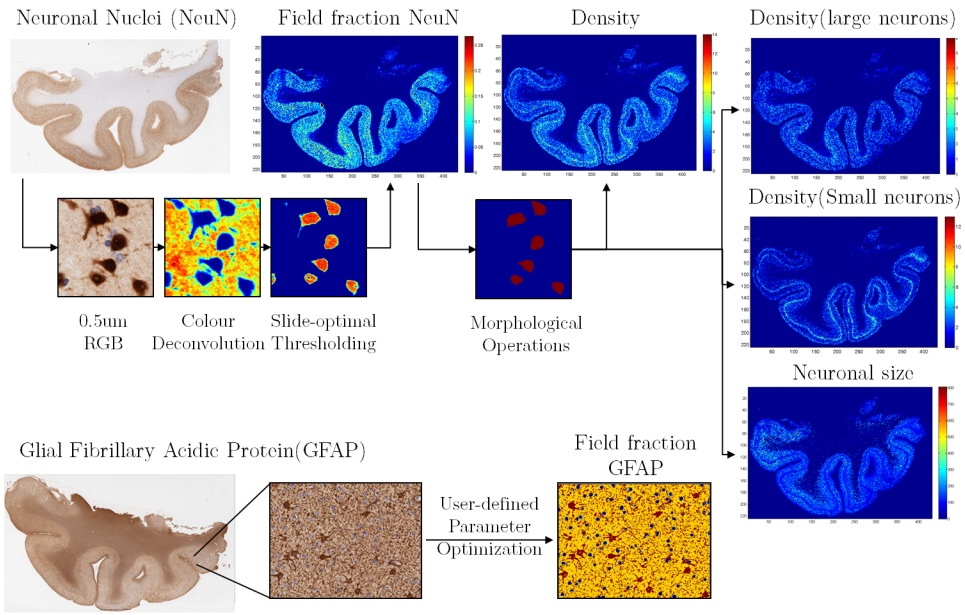
Neuronal Nuclei (NeuN)
Field fraction NeuN
Density
Density(large neurons)
Density(Small neurons)
Neuronal size
0.5um RGB
Colour Deconvolution
Slide-optimal Thresholding
Morphological Operations
Glial Fibrillary Acidic Protein(GFAP)
User-defined Parameter Optimization
Field fraction GFAP

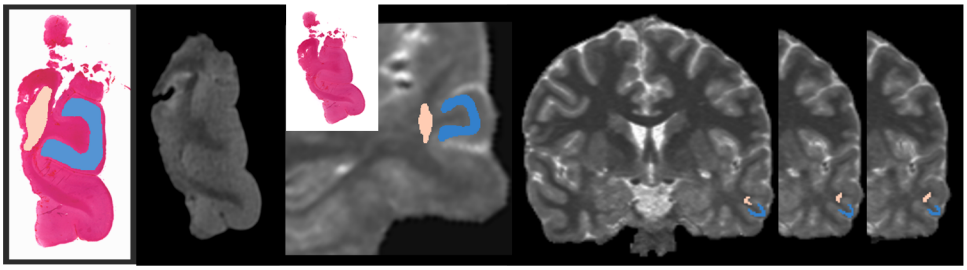

a) b) c) d)

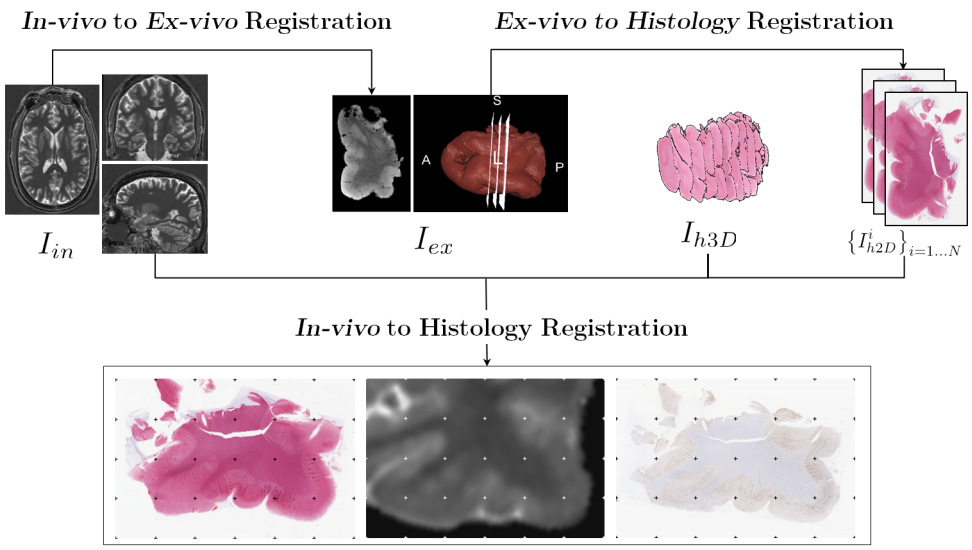
In-vivo to *Ex-vivo* Registration
Ex-vivo to Histology Registration
S
A
L
P
I_{in}
I_{ex}
I_{h3D}
$\{I^i_{h2D}\}_{i=1...N}$
In-vivo to Histology Registration

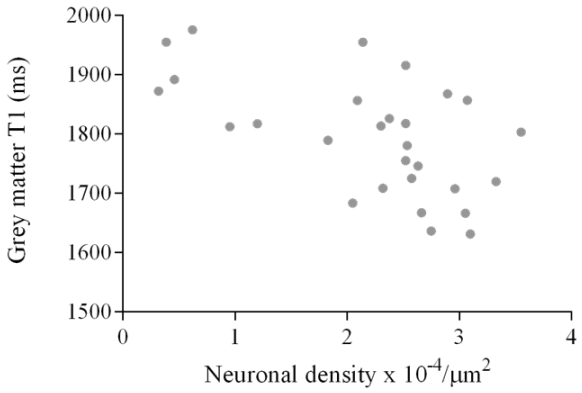
Grey matter T1 (ms)
2000
1900
1800
1700
1600
1500
0
1
2
3
4
Neuronal density x $10^{-4}/\mu m^2$

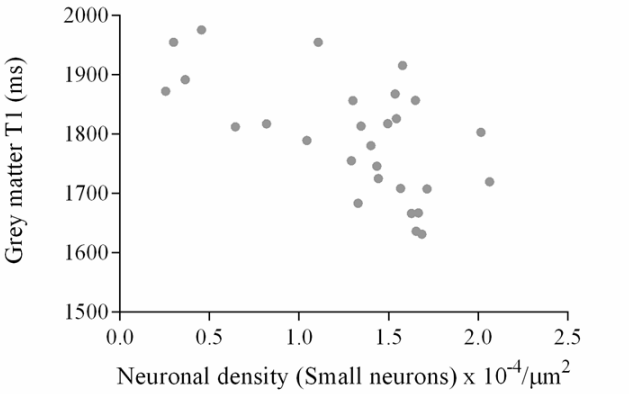
Grey matter T1 (ms)
2000
1900
1800
1700
1600
1500
0.0
0.5
1.0
1.5
2.0
2.5
Neuronal density (Small neurons) x $10^{-4}/\mu m^2$

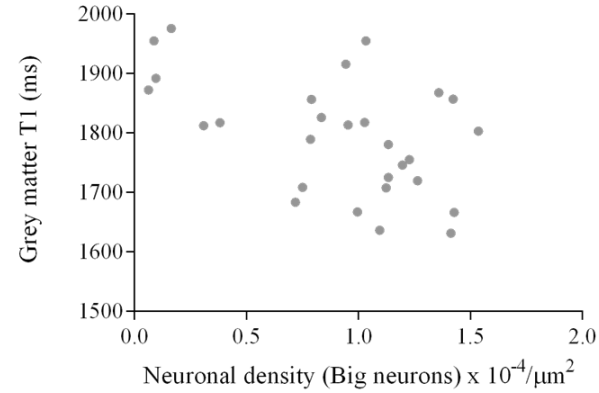
Grey matter T1 (ms)
2000
1900
1800
1700
1600
1500
0.0
0.5
1.0
1.5
2.0
Neuronal density (Big neurons) x $10^{-4}/\mu m^2$

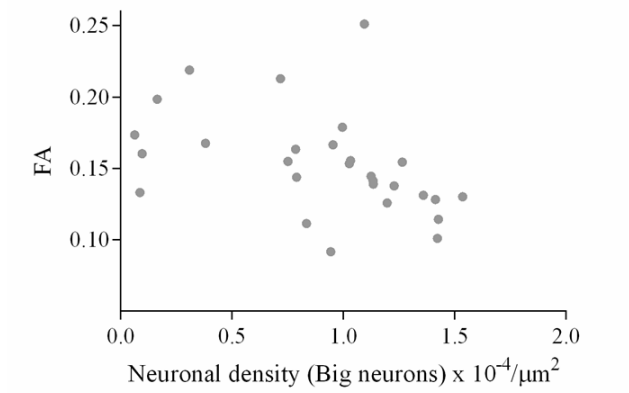
FA
0.25
0.20
0.15
0.10
0.0
0.5
1.0
1.5
2.0
Neuronal density (Big neurons) x $10^{-4}/\mu m^2$

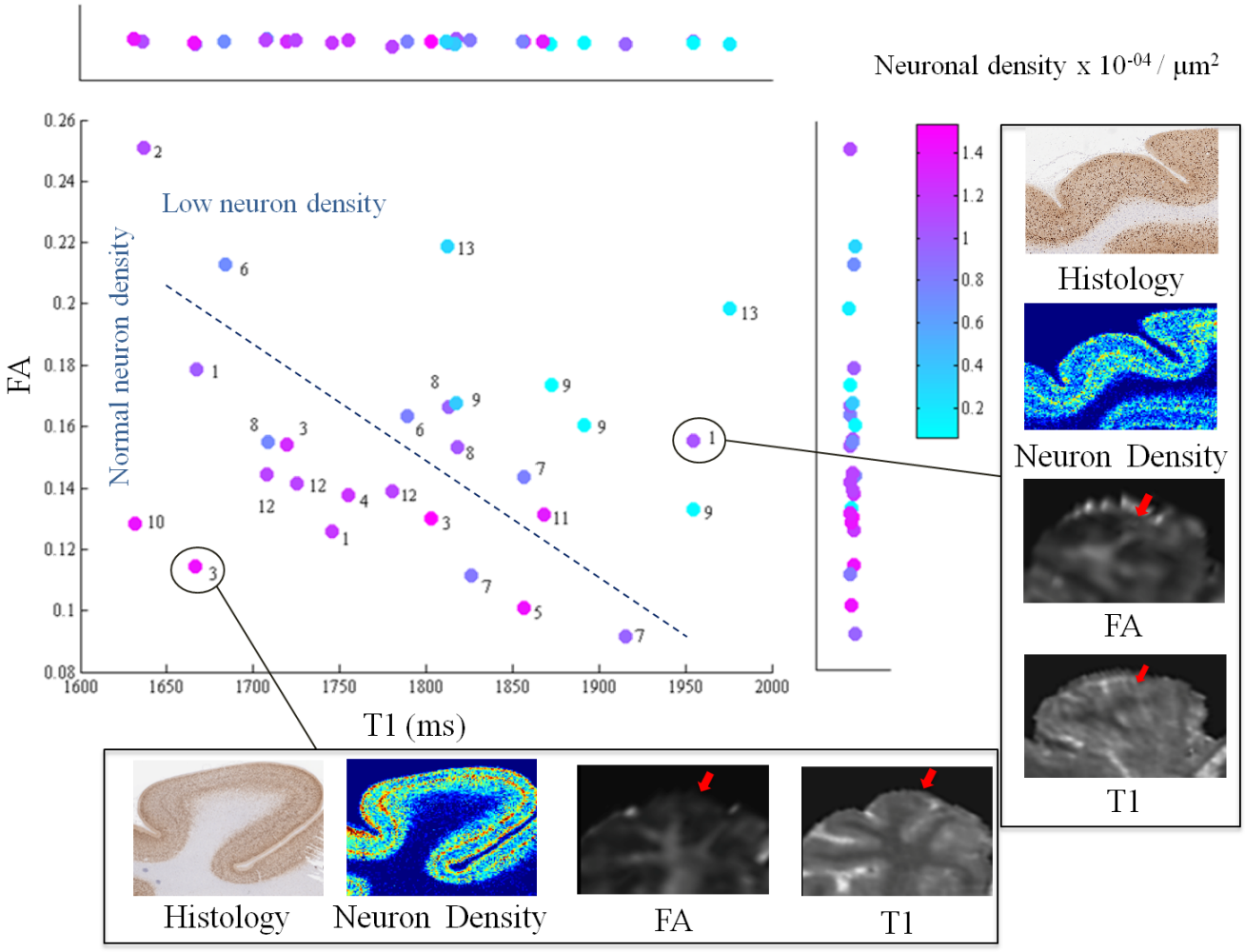
Neuronal density x 10-04 / µm2
Low neuron density
Normal neuron density
FA
T1 (ms)
0.26
0.24
0.22
0.2
0.18
0.16
0.14
0.12
0.1
0.08
1600
1650
1700
1750
1800
1850
1900
1950
2000
1.4
1.2
1
0.8
0.6
0.4
0.2
Histology
Neuron Density
FA
T1
Histology
Neuron Density
FA
T1

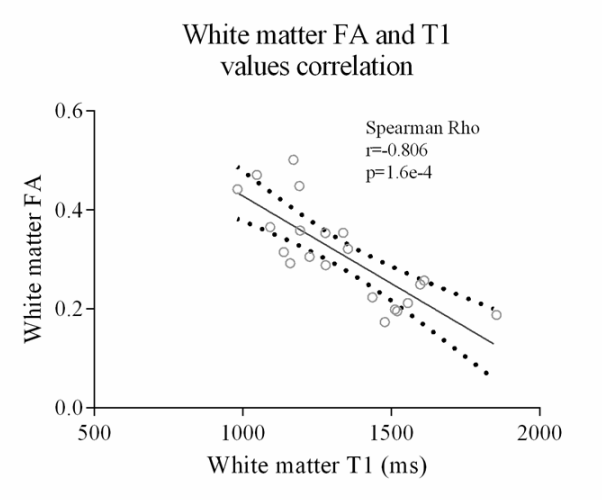
White matter FA and T1 values correlation
Spearman Rho
r=-0.806
p=1.6e-4
White matter FA
White matter T1 (ms)
0.0
0.2
0.4
0.6
500
1000
1500
2000

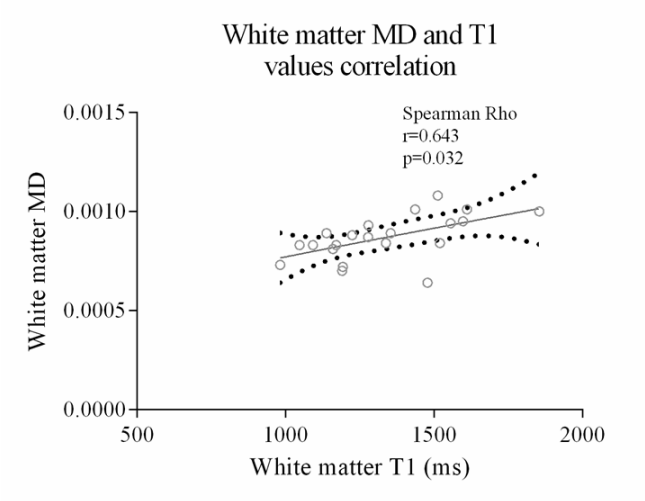
White matter MD and T1 values correlation
Spearman Rho
r=0.643
p=0.032
White matter MD
White matter T1 (ms)
0.0000
0.0005
0.0010
0.0015
500
1000
1500
2000

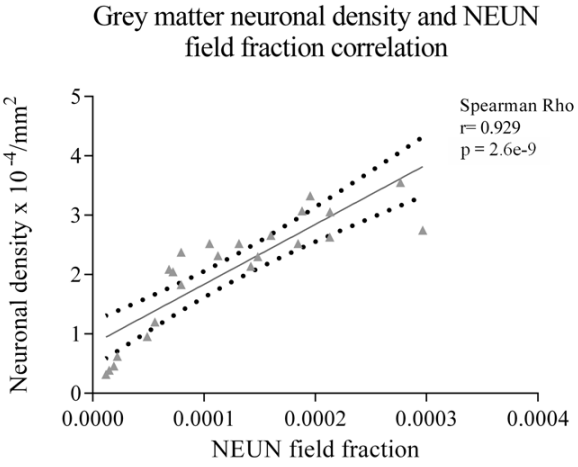
Grey matter neuronal density and NEUN field fraction correlation
Spearman Rho
r= 0.929
p = 2.6e-9
Neuronal density x 10 -4/mm2
NEUN field fraction
0
1
2
3
4
5
0.0000
0.0001
0.0002
0.0003
0.0004

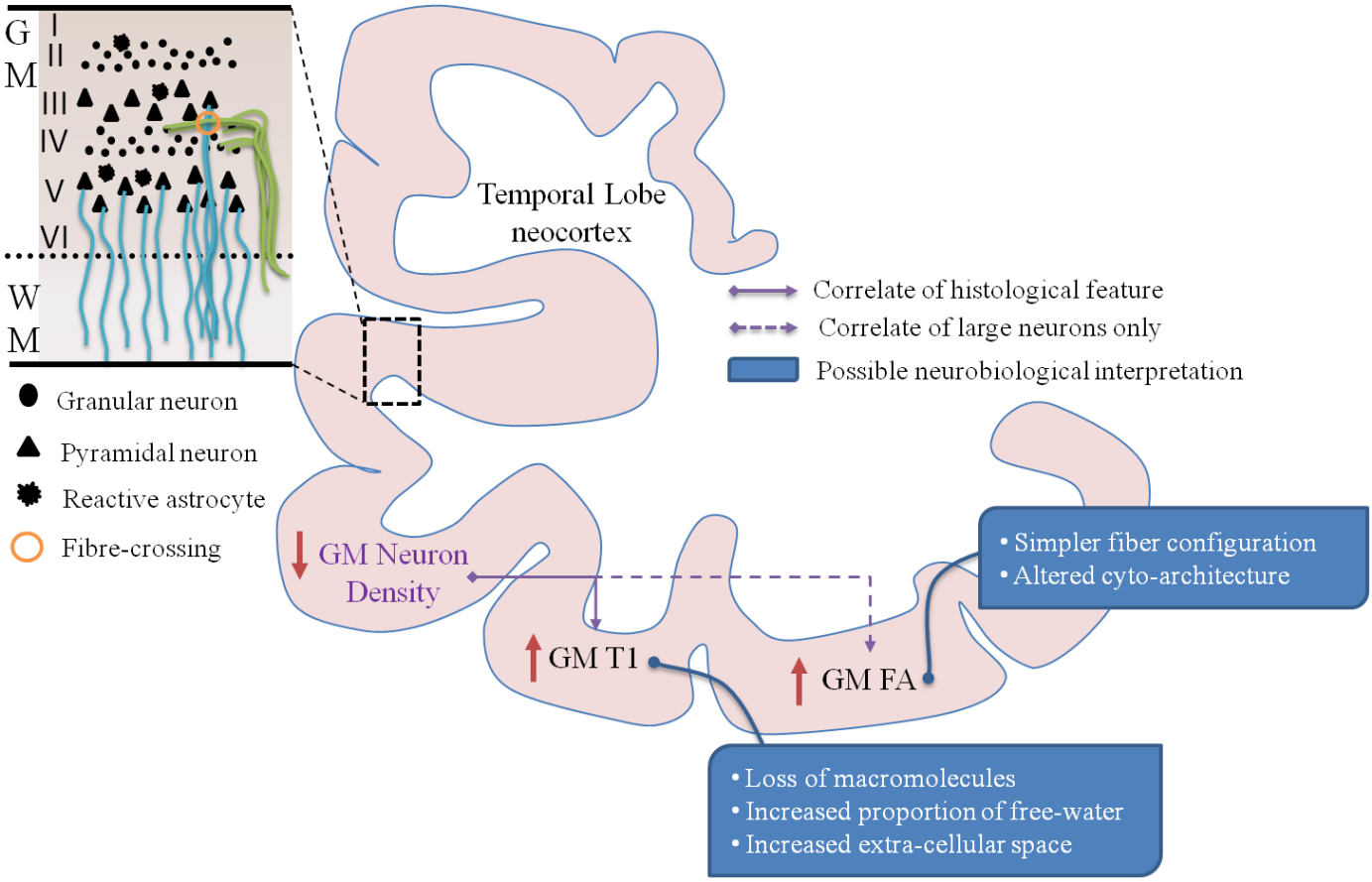
G
M
I
II
III
IV
V
VI
W
M
Granular neuron
Pyramidal neuron
Reactive astrocyte
Fibre-crossing
Temporal Lobe
neocortex
Correlate of histological feature
Correlate of large neurons only
Possible neurobiological interpretation
GM Neuron
Density
GM T1
GM FA
• Simpler fiber configuration
• Altered cyto-architecture
• Loss of macromolecules
• Increased proportion of free-water
• Increased extra-cellular space